PHYSICS OF FLUIDS **26**, 122005 (2014)

Regimes of miscible fluid thread formation in microfluidic focusing sections

Thomas Cubaud[a] and Sara Notaro
Department of Mechanical Engineering, Stony Brook University, New York 11794, USA

(Received 31 March 2014; accepted 24 November 2014; published online 16 December 2014)

We experimentally study the formation and stability of miscible fluid threads made of high-viscosity liquids using hydrodynamic focusing sections. Miscible core annular flows are useful for transporting viscous materials and can be destabilized for enhancing mass transfer. We delineate phase-diagrams of the generation of lubricated threads from low to large viscosity contrasts with various diffusion coefficients. Depending on fluid properties and flow rates of injection, stable microflows are classified into engulfment, thread, and tubing regimes. For low Péclet numbers, we examine thread dynamics when diffusive effects strongly alter basic flow structures and induce new flow configurations, including ultra-diffusive and diffusive instability regimes. Another unstable flow arrangement is investigated for moderate Reynolds numbers where small threads are rapidly destabilized in the inertial flow field of the sheath fluid near the fluid junction. This study provides an overview of stable and unstable flow regimes and their transitions during the formation of miscible viscous fluid filaments in square microchannels. © *2014 AIP Publishing LLC*. [http://dx.doi.org/10.1063/1.4903534]

I. INTRODUCTION

Multiphase flows in microgeometries encompass a wide range of fluid phenomena and find use for a variety of applications, including oil and gas recovery,[1] biomaterial synthesis,[2] and drug discovery.[3] Microfluidic platforms are practical for generating arrays of monodisperse bubbles and droplets when immiscible fluid streams are focused into a single channel.[4–10] When fluids are miscible, it is often desirable to form diffusion gradients[11] or achieve rapid mixing for homogenizing solutions of reagents.[12–14] While turbulent mixing occurs at large Reynolds numbers,[15] miniature flow devices are commonly operated in creeping flow conditions and mixing fluids having similar viscosities requires the development of active and passive methods, such as electrokinetics,[16] piezoelectric elements,[17] oscillatory flows,[18] laminating channels,[19] or wall modifications[20] to essentially increase the fluid interfacial area and reduce diffusional paths. In the case where fluids have large differences in viscosities, efficient blending is particularly challenging due to the constituents' tendency to stratify under flow and form complex velocity and viscosity fields.[21–25] In addition, viscosity-differing fluids can naturally self-lubricate[26] and form viscous threads enveloped in sheaths of less viscous fluids depending on injection scheme and fluid properties.

The control of hydrodynamic instabilities with high-viscosity fluids in microchannels is promising to expand the processing and mixing capabilities of microflow systems to a broad range of thick materials, such as polymers or petroleum. Depending on the type of applications, one may wish to increase the viscosity of a thin fluid by adding a viscosifier or reduce the viscosity of a thick material by adding a thinner. The formation of viscous threads lubricated with low-viscosity solvents offers significant advantages for manipulating thick substances in confined microgeometries. For instance, the folding instability of viscous threads can be precisely adjusted using tailored microfluidic networks to interrogate the influence of viscosity and interfacial tension on the shape and

[a]Author to whom correspondence should be addressed. Electronic mail: thomas.cubaud@stonybrook.edu

dynamics of folds.[27,28] This instability can also be manipulated with electric fields[29] and employed to fabricate crimped microfibers.[30] Other general flow destabilization processes with fluids having large viscosity contrasts include viscous fingering during fluid displacement in porous media[31–33] and shear instabilities of stratified flows.[34–38] For moderate Reynolds numbers, inertial effects can also be harnessed in microfluidic devices and secondary flows be exploited to enhance fluid mixing using curved microchannels[39] or to align particles in a straight channel.[40] In general, it would be useful to develop a unifying picture of the behavior of miscible micro-threads in straight microchannels and characterize the regions in the control parameter space where high-viscosity fluid mixing can be passively enhanced due to hydrodynamic instabilities.

Here, we experimentally study the formation of viscous threads in simple microfluidic focusing sections and provide robust scaling relationships to predict miscible flow transitions between stratified and lubricated states for a broad range of viscosity contrasts. In particular, we show the existence of a diffusive instability for viscous threads convected at small flow rates and we examine the onset of inertial instabilities for moderate Reynolds numbers. We discuss the main features of these original instability patterns and measure the critical thread length before encapsulation and during various destabilization processes. We determine the control parameters that govern steady and unsteady flow regime transitions during miscible fluid transport in square microchannels.

II. EXPERIMENTAL METHODS

Microchannels consist of selectively etched-through silicon wafers of height $h = 250$ μm and borosilicate glasses and are made using standard microfabrication techniques, including microlithography, deep reactive ion etching, and anodic bonding.[41] The focusing section consists of two square channels that intersect at right angles [Fig. 1(a)]. The high-viscosity fluid $L1$ having a viscosity η_1 is injected into the central channel at a flow rate Q_1 and the less viscous fluid $L2$ of viscosity η_2 is symmetrically introduced in the side channels at a total flow rate Q_2. Fluids are injected using syringe pumps and microdevices are placed on top of an inverted microscope equipped with a high-speed camera to analyze flows. To map developing flows near the channel orifice, the origin of the coordinate system is placed at the transition between the central and the observation channels.

Miscible silicone oils of various viscosities are used as model fluids. Since silicone oils differ only by their molecular weight, particular oil pairs are selected to examine microflows with fluids having similar viscosity contrasts $\chi = \eta_1/\eta_2$ but different diffusion coefficients D. The diffusion coefficients D are estimated using Stokes-Einstein law assuming that, at constant temperature, the product $D\eta_2 R$, where R is the molecular hydrodynamic radius of the highly viscous oil $L1$, is essentially constant. Using this argument in conjunction with the oil manufacturer specifications (*Gelest*) yields $D\eta_2\eta_1^{0.34} = K$, where the constant K is determined based on published data for diffusion coefficients D of conventional silicone oils.[42,43] The range of dynamic viscosity contrast χ investigated spans between 10 and 10^4. Experiments are conducted for various thread viscosities η_1 in two different continuous phases, one having a very low viscosity $\eta_2 = 0.49$ cP and the other one having

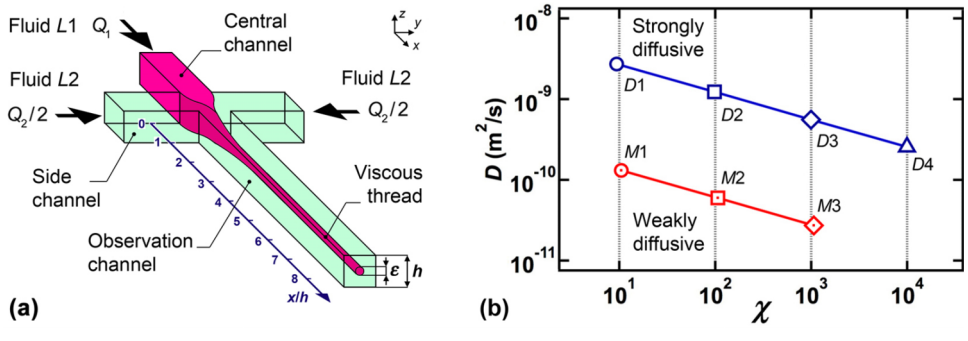

FIG. 1. (a) Schematics of thread formation using a symmetric hydrodynamic focusing section. (b) Evolution of diffusion coefficient with viscosity contrast χ for various fluid pairs.

a medium viscosity $\eta_2 = 4.6$ cP. The Schmidt number $\mathrm{Sc} = \eta_2/(\rho_2 D)$, where ρ_2 is the density of $L2$, is sometimes used to characterize phenomena involving both momentum and mass diffusion processes.[44] Fluid viscosities, diffusion coefficients, and Schmidt numbers are displayed in Table I. Fluid pairs are labeled based on the external fluid viscosity η_2 with "D" for the low-viscosity and strongly diffusive external oil (low Sc) and "M" for the medium-viscosity and weakly diffusive surrounding oil (large Sc). The number in the label indicates the order of magnitude of the viscosity contrast χ [Fig. 1(b)].

This method allows us to compare strongly and weakly diffusive flows for equivalent viscosity contrasts χ. This technique also permits to experimentally decorrelate primary flows that are essentially governed with the flow ratio $\varphi = Q_1/Q_2$ and the viscosity contrast $\chi = \eta_1/\eta_2$ and unstable flows, whose characteristics also depend on the absolute flow rate $Q_1 + Q_2$, the diffusion coefficients D, and the external phase viscosity η_2. The Péclet number $\mathrm{Pe} = (Q_1 + Q_2)/(Dh)$ is convenient for describing systems in the presence of convection and diffusion. In this work, Pe is varied between 2×10^2 and 2×10^6. Inertial phenomena are known to strongly depend on the Reynolds number $\mathrm{Re} = \rho_2(Q_1 + Q_2)/(\eta_2 h)$, which is varied between 10^{-1} and 10^2 in this study.

III. FLOW MAPS

A multitude of regimes are observed depending on flow rates of injection Q_1 and Q_2, absolute viscosities η_1 and η_2, and diffusion coefficients D. To better understand the influence of basic parameters on regime selections, we first compare flow maps between strongly and weakly diffusive fluid pairs ($D3$ and $M3$) having similar viscosity contrast $\chi \sim 10^3$ [Fig. 2].

Steady primary flow patterns are obtained with the fluid pair $M3$ having a small diffusion coefficient D and consist of stratified and lubricated flows, including "tubing," "stable thread," and "engulfment" regimes [Fig. 2(a)]. Over the range of parameters investigated, the flow rate ratio $\varphi = Q_1/Q_2$ is found to control basic regime transition independently of absolute values of Q_1 and Q_2. For a given fluid pair, transitions from a regime to another occur for fixed values of φ. The tubing regime is a stratified flow obtained for large φ and consists of a central strip of $L1$ that occupies most of the channel cross-section and directly contacts top and bottom walls. For lower values of φ, the stable thread regime corresponds to a core-annular flow where $L1$ is fully lubricated by $L2$ and forms a core thread having a nearly uniform velocity profile.[45] The engulfment regime is obtained for very low φ and consists of the low viscosity fluid invading the central channel and locally producing counter flows. Very small threads are typically formed in this regime.

The flow map obtained for the strongly diffusive fluid pair $D3$ offers a more challenging classification as, in addition to base primary flows, three flow regimes, including "ultra-diffusive," "diffusive," and "inertial" instabilities are identified [Fig. 2(b)]. The ultra-diffusive regime is a steady state obtained for very low flow velocities and consists of fluid spatially mixing at short distances near the junction. As the flow rate increases, a periodic instability is seen to alter straight threads into a complex braided structure near the junction. Since such flow patterns are found to occur below a critical flow velocity with fluid pairs having large diffusion coefficients, we infer that basic flow structures are altered due to molecular diffusion and, in consequence, these regimes are referred

TABLE I. Properties of pairs of liquids $L1$ (central stream) and $L2$ (side streams) with corresponding dynamic viscosities η_1 and η_2, viscosity contrast $\chi = \eta_1/\eta_2$, diffusion coefficient D, and Schmidt number $\mathrm{Sc} = \eta_2/(\rho_2 D)$.

Pair	η_1 (cP)	η_2 (cP)	χ	D (m^2/s)	Sc	Symbol
$D1$	4.59×10^0	4.95×10^{-1}	9.2×10^0	2.7×10^{-9}	2.4×10^2	○
$D2$	4.80×10^1	4.95×10^{-1}	9.7×10^1	1.2×10^{-9}	5.4×10^2	□
$D3$	4.86×10^2	4.95×10^{-1}	9.8×10^2	5.6×10^{-10}	1.2×10^3	◇
$D4$	4.87×10^3	4.95×10^{-1}	9.8×10^3	2.6×10^{-10}	2.5×10^3	△
$M1$	4.80×10^1	4.59×10^0	1.0×10^1	1.3×10^{-10}	3.8×10^4	⊙
$M2$	4.86×10^2	4.59×10^0	1.1×10^2	6.0×10^{-11}	8.3×10^4	⊡
$M3$	4.87×10^3	4.59×10^0	1.1×10^3	2.7×10^{-11}	1.9×10^5	◈

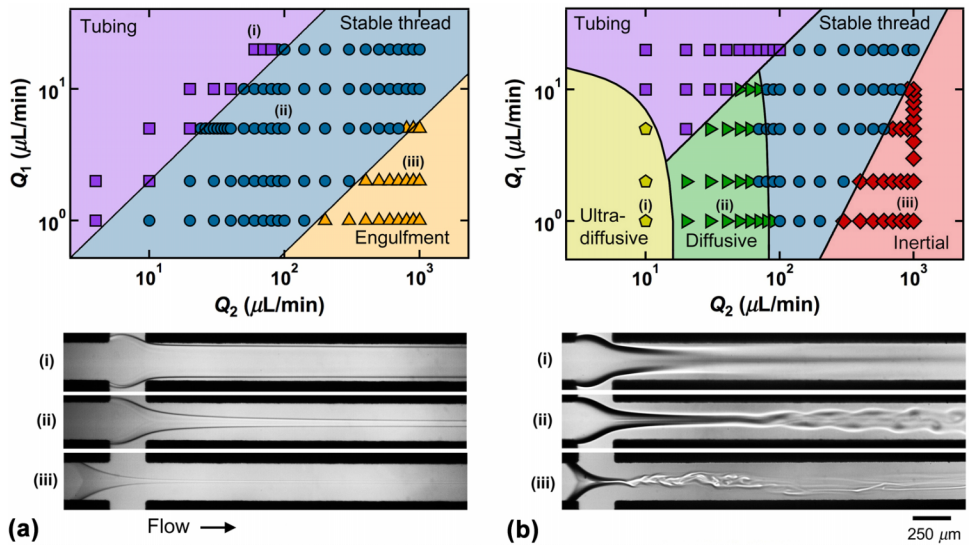

FIG. 2. Weakly and strongly diffusive phase diagrams at large $\chi \sim 10^3$. (a) Basic stable flows obtained with the low diffusivity fluid pair $M3$, flow rates (Q_1, Q_2) are indicated in μl/min, micrographs: (i) tubing (20, 70), (ii) stable thread (5, 100), (iii) and engulfment (2, 800) regimes. (b) Stable and unstable flow regimes for a strongly diffusive fluid pair $D3$, micrographs: (i) ultra-diffusive regime (1, 10), (ii) diffusive instability (1, 40), and (iii) inertial instability (1, 900).

to as "diffusive instabilities." For large injection speeds, the flow at the channel entrance is not fully developed and appears to strongly destabilize small threads above a critical flow velocity. As this remarkable flow behavior is only reached for relatively large Reynolds numbers, we label this regime as "inertial instability." In general, flow instabilities favor the growth of transfer surfaces and should in principle enhance the overall mixing process. The transition between stable and unstable flow patterns depends on dimensionless quantities such as the Péclet and Reynolds numbers, which in turn depend on absolute flow and fluid properties.

IV. BASIC FLOW REGIMES

To delineate the major features of miscible fluid thread formation mechanisms, we first focus on regimes associated with basic thread formation for low Re (strongly laminar) and high Pe (non-diffusive). A fundamental property of viscosity-stratified flows in ducts is the possibility for low-viscosity fluids to envelop high-viscosity fluids and produce lubricated viscous threads. The conditions required to initiate high-viscosity flow separation from the walls, however, are poorly understood. Here, steady, miscible contact lines between fluids and walls are apparent in experimental micrographs and adopt a nearly triangular shape that expands in the outlet channel [Fig. 3(a)]. The contact point where miscible contact lines merge at the solid walls is used to measure the thread formation length L_S. Downstream of the contact point, data show the persistence of a thin contact line aligned with the flow direction, which suggests that a small portion of $L1$ is still in contact with the walls. This line, however, quickly blends with the surrounding fluid yielding a fully lubricated thread.

The stable thread formation length L_S is a useful parameter to characterize base flow regimes. In particular, L_S diverges for finite values of φ near regime changes [Fig. 3(b)]. For instance, for the viscosity contrast $\chi \sim 10^3$, the stable/engulfment transition is estimated as $\varphi_{Eng} \sim 7.1 \times 10^{-3}$ and the stable/tubing transition at $\varphi_{Tub} \sim 2.9 \times 10^{-1}$. In the engulfment regime, very thin threads are formed and L_S offers a simple quantitative parameter to define this regime. In most of the stable thread flow regimes, the initial thread length L_S is found to be directly proportional to the flow rate ratio φ such as $L_S/h = k\varphi$, where the coefficient k depends on the viscosity contrast χ according to $k = 3.3 + 1.6 \times 10^{-2}\chi$ [Fig. 3(b)-inset]. For very large $\chi \gg 1$, experimental data suggest the asymptotic scaling $L_S \sim \chi\varphi$ for the thread formation length.

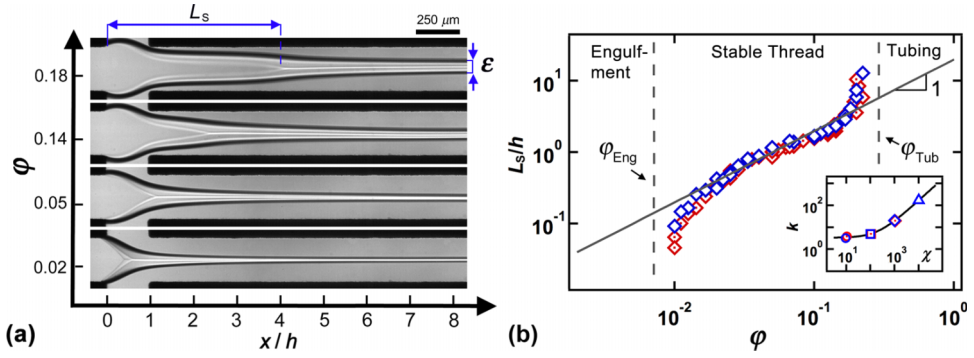

FIG. 3. Formation length L_S of stable threads. (a) Micrographs showing the development of L_S as a function of the flow rate ratio φ, fluid pair: $D3$. (b) Formation length L_S as a function of φ for $\chi \sim 10^3$ transitions, $\varphi_{Eng} = 7.1 \times 10^{-3}$, $\varphi_{Tub} = 2.9 \times 10^{-1}$, solid line: $L_S/h = 19.8\varphi$, fluid pairs: $D3$ (◇) and $M3$ (◈). Inset: evolution of prefactor k with viscosity ratio χ, solid line: $k = 3.3 + 1.6 \times 10^{-2}\chi$.

The width of the central stream ε is observed to significantly decrease in the area around the separation point of $L1$ from the walls before ε reaches a nearly constant value further downstream. The thread diameter ε is measured in the observation channel using grayscale analysis of light intensity normal to the thread flow direction [Fig. 4(a)]. Here, we restrict our measurements to the stable thread regime in the absence of significant diffusive and inertial effects. The diameter is computed between the two points of minimal intensity around the thread and remains constant in our field of view for $x/h \geq 6$. Although very small threads can also be formed in the engulfment regime, the spatial resolution of this series of experiments limits our measurements for $\varepsilon/h \leq 5 \times 10^{-2}$ as it corresponds to a threshold value for the uncertainty error of 20%. Previous work showed that in the limit of $\chi \gg 1$ and $\varepsilon/h \ll 1$, the theoretical expression $\varepsilon/h = (\varphi/2)^{1/2}$, which is valid for core-annular flow in a circular duct, holds good agreement with measured thread widths in square microchannels.[45] Here, data are fitted with the function $\varepsilon/h = \alpha\varphi^{1/2}$, where the coefficient α reaches a plateau value of $\alpha_S = 2^{-1/2}$ for $\chi \geq 10^2$ [Fig. 4(b)]. For $\chi \sim 10$, values of α are considerably lower than α_S as the relative viscosity between fluids is too low to produce fully lubricated threads having a uniform velocity profile.

The critical flow rate ratios φ_{Tub} and φ_{Eng} at which basic flow transitions occur are useful for determining the range of stable thread sizes available as a function of constituents' viscosities. Basic scaling for the transition curves are determined according to $\varphi_{Tub} \sim 2\chi^{-0.3}$ for the tubing/stable thread transition and $\varphi_{Eng} \sim 0.27\chi^{-0.6}$ for the engulfment/stable transition [Fig. 4(c)]. The tubing/thread transition corresponds to the lubrication transition in compact microgeometries between stratified and lubricated flows. In microfluidic chambers,[46] a similar trend was found for the lubrication transition of folding threads with a more pronounced influence of the viscosity contrast according to

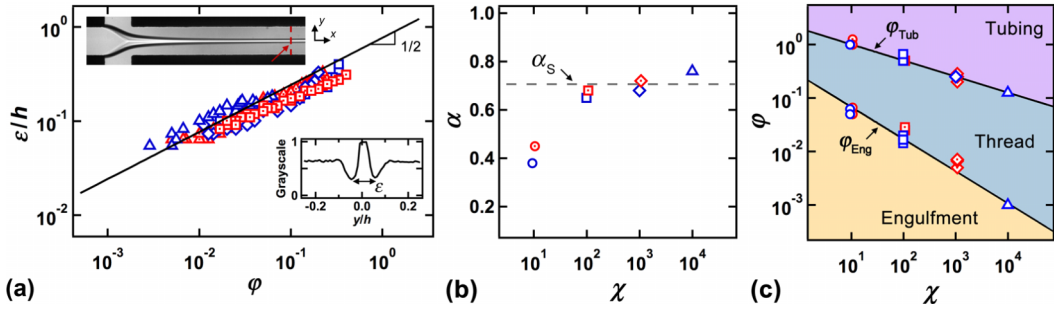

FIG. 4. (a) Evolution of normalized stable thread diameter ε/h with the flow rate ratio φ for χ ranging between 10^2 and 10^4, top inset: micrograph with arrow to indicate location of grayscale analysis, bottom inset: example of grayscale profile used to measure ε. (b) Variation of coefficient α with viscosity contrast χ, dashed line: $\alpha_S = 2^{-1/2}$ (c) Phase-diagram for base flow regimes with flow rate ratio φ vs. viscosity contrast χ. Solid lines: tubing/thread transition, $\varphi_{Tub} = 2\chi^{-0.3}$, engulfment/thread transition, $\varphi_{Eng} = 0.27\chi^{-0.6}$. Symbols for fluid pairs are indicated in Table I.

$\varphi = 1.8\chi^{-0.6}$. Here, data also show that, as χ increases, the conditions for production of small steady threads improve due to a better resistance to engulfment of the less viscous fluid in the central channel. The generation of larger threads, however, is limited at large χ due to the presence of the tubing regime.

V. UNSTABLE FLOW REGIMES

In this section, we examine the main features of unstable flow regimes that are characterized by a significant modification of the basic flow structures. Information gained about the influence of the flow rate ratio φ and the viscosity contrast χ is key for the determination of steady lubricated flow states. Here, the flow stability is probed for a variety of diffusion coefficients D and flow velocities $J = (Q_1 + Q_2)/h^2$. In general, fluid pairs associated with large diffusion coefficients D (i.e., small Péclet numbers Pe) are prone to diffusion-induced flow instabilities. Similarly, when the lubricant viscosity η_2 is small, the development of inertial instabilities is facilitated as moderate Reynolds numbers are reached, Re ~ O(2). In practice, fluid pairs having a low viscosity fluid also have a large diffusion coefficient and therefore, fluid pairs of low Schmidt numbers Sc exhibit both diffusive instabilities for small flow rates and inertial instabilities for large flow rates. Flow regimes are classified based on their optical signatures, as their generic features are readily identifiable with a visual inspection of micrographs.

A. Diffusive regimes

Diffusive instabilities are observed with fluid pairs $D1$ to $D4$ and are classified using the Péclet number Pe [Fig. 5(a)]. In general, diffusive regime transitions are found to be relatively insensitive to the viscosity ratio χ and the flow rate ratio φ. In Fig. 5, we do not include diffusive transitions with the tubing regime. For large Péclet numbers $\mathrm{Pe} > \mathrm{Pe_S}$, where $\mathrm{Pe_S} \approx 10^4$, stable threads are formed and display similar characteristics, including diameter ε and formation length L_S, as those produced with the weakly diffusive fluid pairs $M1$ to $M3$ [Fig. 5(b) (i)] As Pe is lowered below $\mathrm{Pe_S}$, threads that are initially stable near the observation channel orifice are seen to destabilize at a certain distance downstream and highly complex viscous structures are produced in the observation channel [Fig. 5(b) (ii)]. This intriguing regime is observed for moderate Péclet numbers when $\mathrm{Pe} > \mathrm{Pe_D}$, where $\mathrm{Pe_D} \approx 1.5 \times 10^3$. For low Péclet numbers $\mathrm{Pe} < \mathrm{Pe_D}$, the ultra-diffusive flow regime is characterized with a thread progressively blending with the surrounding fluid [Fig. 5(b) (iii)]. Although the fluid/fluid interface appears sharp near the fluid section, for very small injection speeds, i.e., for long residence times, the grayscale gradient at the interface between the thread and the external liquid diminishes along the flow direction, and eventually the thread is no longer distinguishable from the surrounding fluid.

By contrast to the steady ultra-diffusive regime, the diffusive regime shows periodical oscillations at specific distances from the fluid junction. For a given fluid pair, the destabilization length L_{Diff} can

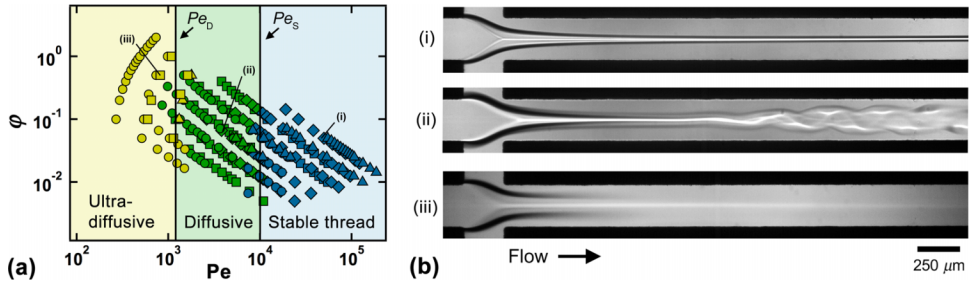

FIG. 5. (a) Phase diagram of diffusive instabilities with flow rate ratio φ and Péclet number Pe, the tubing regime is omitted. Solid lines represent transitions between ultra-diffusive/diffusive instabilities, $\mathrm{Pe_D} \approx 1.5 \times 10^3$, and diffusive/stable thread regimes, $\mathrm{Pe_S} \approx 10^4$. Symbols are indicated in Table I. (b) Micrographs with flow rates (Q_1, Q_2) indicated in μl/min: (i) stable thread (20, 500), fluid pair $D3$; (ii) Diffusive instability (2, 30), fluid pair $D3$; and (iii) ultra-diffusive regime (2, 10), fluid pair $D2$.

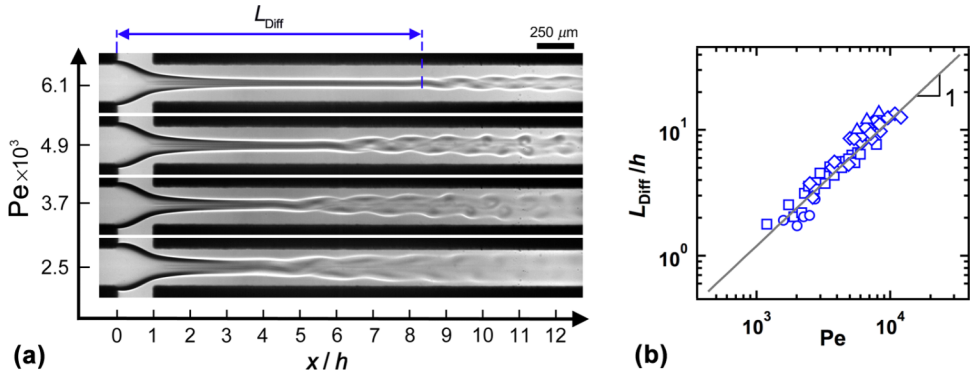

FIG. 6. Diffusive destabilization length L_{Diff}. (a) Micrographs showing the evolution of L_{Diff} for various Péclet number Pe, fluid pair $D3$. (b) Evolution of normalized destabilization length with the Péclet number for diffusive fluid pairs, solid line: $L_{\mathrm{Diff}}/h = 1.2 \times 10^{-3}\mathrm{Pe}$. Symbols are indicated in Table I.

be adjusted with the total flow rate of injection, i.e., average flow velocity, which is non-dimensionally represented with the Péclet number Pe [Fig. 6(a)]. The average thread length L_{Diff} before destabilization is experimentally determined by superimposing micrographs from high-speed movies onto a composite image and measuring the location at which the combined thread diameter ε increases along the flow direction. Data show that the diffusion length L_{Diff} is directly proportional to the Péclet number Pe according to $L_{\mathrm{Diff}}/h = 1.2 \times 10^{-3}\mathrm{Pe}$ for fluid pairs $D1$ to $D4$ [Fig. 6(b)]. Although a detailed investigation of this particular regime is beyond the scope of this article, experiments show that the thread experiences some kind of a "diffusive coiling" that leads to the formation of a central fluid structure having an effective diameter that increases along the flow direction, which suggests that mixing is locally enhanced near the thread. We note that the upper limit for the threshold Péclet number $\mathrm{Pe_S} \approx 10^4$ is somewhat arbitrary since the field of view corresponds to the portion of the channel after the junction and extends over a distance $x/h \sim 12$.

B. Inertial regime

Dynamic interactions between the forming slender viscous structure and the developing inertial flow field near the observation channel entrance can significantly alter thread structural integrity for moderate Reynolds numbers $\mathrm{Re} = \rho_2(Q_1 + Q_2)/(\eta_2 h)$. As the full development of the laminar flow velocity profile requires an entry length $L/h \sim 8 \times 10^{-2}$ Re from the channel entrance,[47] which is located at $x = h$, the region downstream the fluid junction (where destabilization occurs) becomes significant with respect to thread formation ($L > h$) for moderate Reynolds numbers $\mathrm{Re} \geq 13$. Such regimes are obtained with fluid pairs having a low external viscosity η_2, such as pairs $D1$ to $D4$.

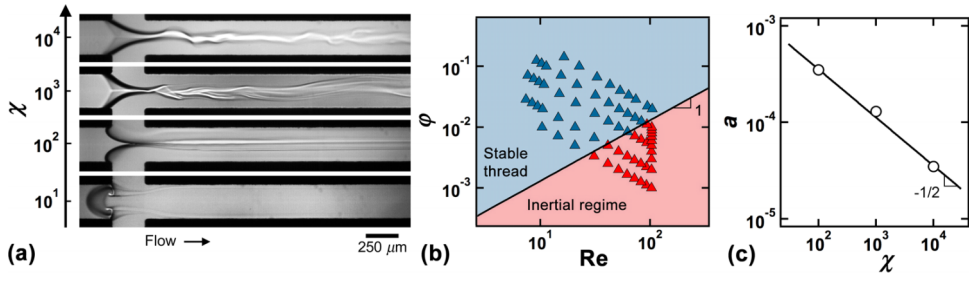

FIG. 7. Inertial instabilities during miscible thread formation. (a) Micrographs showing inertial thread destabilizations for viscosity contrasts χ ranging between 10^1 and 10^4 at fixed flow rates $Q_1 = 1$ and $Q_2 = 10^3$ μl/min, $\varphi = 10^{-3}$, all diffusive fluid pairs, Re ~ 103. (b) Phase-diagram of inertial instabilities based on flow rate ratio φ and Reynolds number Re for viscosity contrast $\chi \sim 10^3$, fluid pair $D3$, solid line: $\varphi = a\mathrm{Re}$ with $a = 1.3 \times 10^{-4}$. (c) Evolution of prefactor a as a function of viscosity contrast χ, solid line: $a = 3.5 \times 10^{-3}\chi^{-1/2}$.

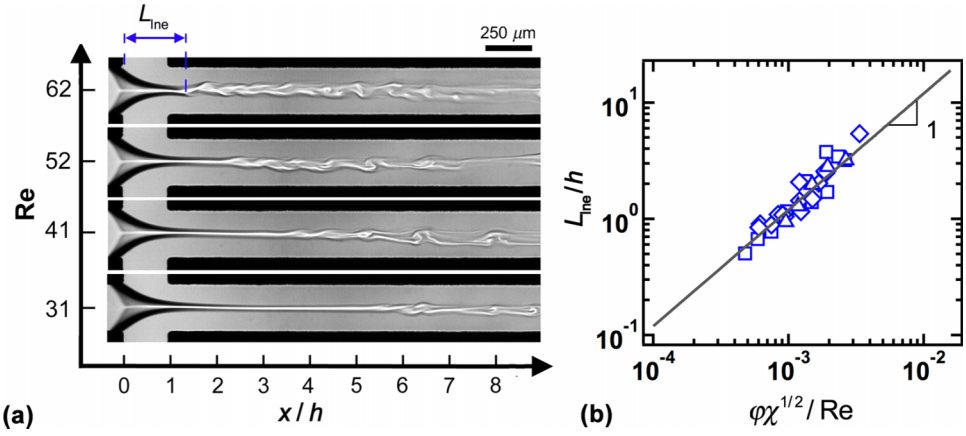

FIG. 8. Evolution of inertial destabilization length L_{Ine}. (a) Micrographs showing the decrease of L_{Ine} with the Reynolds number Re. (b) Scaled inertial thread length L_{Ine}/h as function of dimensionless parameter $\varphi\chi^{1/2}$/Re, solid line: $L_{Ine}/h = 1.2 \times 10^3 \varphi\chi^{1/2}$/Re.

A range of thread behavior is obtained depending on Reynolds numbers Re, viscosity contrasts χ, and flow rate ratios φ. For instance, for fixed Re $\sim 10^2$ and $\varphi = 10^{-3}$, threads appear more resistant to deformation as the viscosity contrast χ increases [Fig. 7(a)]. For low $\chi \sim 10$, a curious inertial engulfment regime with sporadic formation of two rolled-up viscous filaments in the central inlet channel is observed while threads are distorted to different degrees for larger $\chi \geq 10^2$. To classify unstable thread regimes, we inspect flow morphologies in the field of view close to the junction. The neutral curve for the onset of inertial instabilities is found to depend on the flow rate ratio (i.e., thread diameters) for a given Re according to the relationship $\varphi = a$Re, where the coefficient scales as $a \sim b\chi^{-1/2}$, with $b = 3.5 \times 10^{-3}$ [Figs. 7(b) and 7(c)]. The transition between laminar and inertial thread regimes on the phase-diagram reveals that, on the one hand, threads with large sizes ε are more resistant for similar Re, and on the other hand, threads are more resistant to inertial disturbance for large χ. Highly viscous threads in inertial flow fields below criticality are marginally stable with intermittent destabilization processes that are quickly convected for large Re.

As the flow velocity increases, the location at which a thread is destabilized is observed to move toward the fluid junction. To investigate this phenomenon, the stable thread length is denoted by L_{Ine} and digitally measured for various Re using superimposed images from experimental micrographs [Fig. 8(a)]. To capture the influence of flow and fluid properties, the scaling found for inertial instabilities' transitions $\varphi \sim \text{Re}\chi^{-1/2}$ is useful for predicting the thread inertial length L_{Ine} for a wide range of viscosity contrast χ, which shows that, in accordance with experimental data, this length scales as $L_{Ine}/h = 1.2 \times 10^3 \varphi\chi^{1/2}$/Re [Fig. 8(b)].

VI. CONCLUSIONS

In this work, we experimentally study the formation of highly viscous threads in symmetric hydrodynamic focusing sections. The basic flow patterns, including tubing, stable thread, and engulfment regimes, are characterized as a function of viscosity contrast χ and flow rate ratio φ. Methods based on scaling laws are developed to predict the shape of lubricated, highly viscous streams and the operating range of stable thread formation is determined for a large range of fluid viscosities, diffusivities, and flow rates. For low Péclet numbers Pe $< 1.5 \times 10^3$, we reveal the presence of a steady ultra-diffusive instability, while for moderate Pe $< 10^4$, a diffusive instability modifies the thread structure with an apparent helicoidal motion that develops at determined locations along the flow. For a given fluid pair, the thread length before destabilization is found to increase with the multiphase superficial velocity $J = (Q_1 + Q_2)/h^2$. For larger velocities, moderate Reynolds numbers Re $\sim 10^2$ are attained and inertial instabilities strongly distort small threads in the external developing velocity field. In this regime, the thread destabilization length is inversely proportional to the superficial velocity J.

Future directions include the detailed examination of diffusive and inertial instabilities and the determination of their convective/absolute nature in the parameter space within the context of hydrodynamic instabilities.[48–50] Indeed, although the linear relationship between thread destabilization length and flow velocity J for the diffusive instability suggests that disturbances are swept away with the flow in a fashion similar to a convective instability, a comprehensive analysis of the system response to externally imposed disturbances would provide fundamental insights to settle the question relative to the nature of this instability. Comparably, besides the fact that the destabilization length decreases with J for inertial instabilities, which hints at the presence of an absolute instability with perturbations invading the flow domain, an advanced stability analysis through examination of spatiotemporal evolutions of waves would advance our understanding of these microflow phenomena. Another important expansion of this work is rooted in the development of experimental methods for the quantification of the fluid mixing efficiency resulting from various thread destabilization processes. Diffusive instabilities of viscous core-annular flows provide a means for blending fluids at low flow rates based on emerging properties of lubricated and stratified microflows. Conversely, inertial instabilities show promises for the continuous mixing of minute amounts of viscous material into a low-viscosity fluid at high flow rates. Overall, the phenomenon of thin stream destabilization at a certain distance from the channel inlet in pipe flows is reminiscent of the original Reynolds' experiment for the existence of a critical velocity for turbulent flows.[51] In this work, we vary the viscosity of a fluid "vein" and show that a thread becomes more resistant to the inertial disturbances of the external flow field as its internal viscosity increases. This result is in good qualitative agreement with the notion that high-viscosity fluids are more solid-like. Numerical simulations would provide additional information on the evolution of local velocity profiles in conjunction with dynamic variations of viscosity as well as into the influence of streamlines curvature on developing flows in hydrodynamic focusing sections at moderate Re. In general, this work shows that the manipulation of viscous threads via steady flow rates of injection and channel geometry offers a promising hydrodynamic method for passively enhancing mixing between viscous materials at the microscale.

ACKNOWLEDGMENTS

This material is based on work supported by the National Science Foundation under Grant No. CBET-1150389.

[1] J. Bear, *Dynamics of Fluids in Porous Media* (Elsevier Publication Co., New York, 1972).
[2] Y. Song, A. Sauret, and H. C. Shum, "All-aqueous multiphase microfluidics," Biomicrofluidics **7**, 061301 (2013).
[3] P. S. Dittrich and A. Manz, "Lab-on-a-chip: Microfluidics in drug discovery," Nat. Rev. Drug Discovery **5**, 210 (2006).
[4] S. L. Anna, N. Bontoux, and H. A. Stone, "Formation of dispersions using 'flow focusing' in microchannels," Appl. Phys. Lett. **82**, 364 (2003).
[5] N. Dietrich, S. Poncin, N. Midoux, and H. Z. Li, "Bubble formation dynamics in various flow-focusing microdevices," Langmuir **24**, 13904 (2008).
[6] G. F. Christopher and S. L. Anna, "Microfluidic methods for generating continuous droplet streams," J. Phys. D: Appl. Phys. **40**, R319 (2007).
[7] T. Cubaud and T. G. Mason, "Capillary threads and viscous droplets in square microchannels," Phys. Fluids **20**, 053302 (2008).
[8] S. Y. Teh, R. Lin, L. H. Hung, and A. P. Lee, "Droplet microfluidics," Lab Chip **8**, 198 (2008).
[9] C. N. Baroud, F. Gallaire, and R. Dangla, "Dynamics of microfluidic droplets," Lab Chip **10**, 2032 (2010).
[10] B. M. Jose and T. Cubaud, "Formation and dynamics of partially wetting droplets in square microchannels," RSC Adv. **4**, 14962 (2014).
[11] S. Kim, H. J. Kim, and N. L. Jeon, "Biological applications of microfluidic gradient devices," Integr. Biol. **2**, 584 (2010).
[12] J. B. Knight, A. Vishwanath, J. P. Brody, and R. H. Austin, "Hydrodynamic focusing on a silicon chip: Mixing nanoliters in microseconds," Phys. Rev. Lett. **80**, 3863 (1998).
[13] J. M. Ottino and S. Wiggins, "Introduction: Mixing in microfluidics," Philos. Trans. R. Soc., London A **362**, 923 (2004).
[14] C. Y. Lee, C. L. Chang, Y. N. Wang, and L. M. Fu, "Microfluidic mixing: A review," Int. J. Mol. Sci. **12**, 3263 (2011).
[15] D. J. Tritton, *Physical Fluid Dynamics* (Oxford University Press Inc., New York, 1988).
[16] S. M. Shin, I. S. Kang, and Y.-K. Cho, "Mixing enhancement by using electrokinetic instability under time-periodic field," J. Micromech. Microeng. **15**, 455 (2005).
[17] S. Wang, X. Huang, and C. Yang, "Mixing enhancement for high viscous fluids in a microfluidic chamber," Lab Chip **11**, 2081 (2011).
[18] F. Bottausci, I. Mezic, C. D. Meinhart, and C. Cardonne, "Mixing in the shear superposition micromixer: Three-dimensional analysis," Philos. Trans. R. Soc., A **362**, 1001 (2004).

[19] D. S. Kim, S. H. Lee, T. H. Kwon, and C. H. Ahn, "A serpentine micromixer combining splitting/recombination and advection," Lab Chip **5**, 739 (2005).
[20] A. D. Stroock, S. K. W. Dertinger, A. Ajdari, I. Mezic, H. A. Stone, and G. M. Whitesides, "Chaotic mixer for microchannels," Science **295**, 647 (2002).
[21] H. M. Xia, Z. P. Wang, Y. X. koh, and K. T. May, "A microfluidic mixer with self-excited 'turbulent' fluid motion for wide viscosity ratio applications," Lab Chip **10**, 1712 (2010).
[22] Q. Cao, A. L. Ventresca, K. R. Sreenivas, and A. K. Prasad, "Instability due to viscosity stratification downstream of a centerline injector," Can. J. Chem. Eng. **81**, 913 (2003).
[23] B. Selvam, S. Merk, R. Govindarajan, and E. Meiburg, "Stability of miscible core-annular flows with viscosity stratification," J. Fluid. Mech. **592**, 23 (2007).
[24] K. C. Sahu, H. Ding, P. Valluri, and O. K. Matar, "Linear stability analysis and numerical simulation of miscible two-layer channel flow," Phys. Fluids **21**, 042104 (2009).
[25] M. d'Olce, J. Martin, N. Rakotomalala, D. Salin, and L. Talon, "Pearl and mushroom instability patterns in two miscible fluids' core annular flows," Phys. Fluids **20**, 024104 (2008).
[26] D. D. Joseph and Y. Y. Renardy, *Fundamentals of Two-Fluid Dynamics. Part I: Mathematical Theory and Applications* (Springer-Verlag, New York, 1993).
[27] T. Cubaud, B. M. Jose, and S. Darvishi, "Folded micro-threads: Role of viscosity and interfacial tension," Phys. Fluids **23**, 042002 (2011).
[28] S. Darvishi and T. Cubaud, "Formation of capillary structures with highly viscous fluids in plane microchannels," Soft Matter **8**, 10658 (2012).
[29] Y. Song, Z. Liu, T. Kong, and H. C. Shum, "Manipulation of viscous all-aqueous jets by electrical charging," Chem. Commun. **49**, 1726 (2013).
[30] J. K. Nunes, H. Constantin, and H. A. Stone, "Microfluidic tailoring of the two-dimensional morphology of crimped microfibers," Soft Matter **9**, 4227 (2013).
[31] G. M. Homsy, "Viscous fingering in porous media," Annu. Rev. Fluid Mech. **19**, 271 (1987).
[32] E. Lajeunesse, J. Martin, N. Rakotomalala, D. Salin, and Y. C. Yortsos, "Miscible displacement in a Hele-Shaw cell at high rates," J. Fluid Mech. **398**, 299 (1999).
[33] B. Jha, L. Cueto-Felgueroso, and R. Juanes, "Quantifying mixing in viscously unstable porous media flows," Phys. Rev. E **84**, 066312 (2011).
[34] C. S. Yih, "Instability due to viscosity stratification," J. Fluid Mech. **27**, 337 (1967).
[35] C.-H. Li, "Instability of three-layer viscous stratified flow," Phys. Fluids **12**, 2473 (1969).
[36] R. Govindarajan and K. C. Sahu, "Instabilities in viscosity-stratified flow," Annu. Rev. Fluid Mech. **46**, 331 (2014).
[37] P. Valluri, L. Ó. Náraigh, H. Ding, and P. D. Spelt, "Linear and nonlinear spatio-remopral instability in laminar two-layer flows," J. Fluid Mech. **656**, 458 (2010).
[38] L. Ó. Náraigh, P. Valluri, T. P. Scott, I. Bethune, and P. D. Spelt, "Linear instability, nonlinear instability and ligament dynamics in three-dimensional laminar two-layer liquid-liquid flows," J. Fluid Mech. **750**, 464 (2014).
[39] D. D. Carlo, "Inertial microfluidics," Lab Chip **9**, 3038 (2009).
[40] J. Zhou and I. Papautsky, "Fundamentals of inertial focusing in microchannels," Lab Chip **13**, 1121 (2013).
[41] M. J. Madou, *Fundamentals of Macrofabrication and Nanotechnology* (CRC Press, Boca Raton, FL, 2012), Vol. 2.
[42] N. Rashidnia, R. Balasubramaniam, J. Kuang, P. Petitjeans, and T. Maxworthy, "Measurement of the diffusion coefficient of miscible fluids using both interferometry and Wiener's method," Int. J. Thermophys. **22**, 547 (2001).
[43] T. Cubaud and T. G. Mason, "Formation of miscible fluid microstructures by hydrodynamic focusing in plane geometries," Phys. Rev. E **78**, 056308 (2008).
[44] S. P. Vanka and C. M. Winkler, "Numerical study of scalar mixing in curved channels at low Reynolds numbers," AIChE J. **50**, 2359 (2004).
[45] T. Cubaud and T. G. Mason, "High-viscosity fluid threads in weakly diffusive microfluidic systems," New J. Phys. **11**, 075029 (2009).
[46] S. Darvishi and T. Cubaud, "Lubrication of highly viscous core-annular flows in microfluidic chambers," J. Fluids Eng. **133**, 031203 (2011).
[47] P.-F. Hao, F. He, and K.-Q. Zhu, "Flow characteristics in a trapezoidal silicon microchannel," J. Micromech. Microeng. **15**, 1362 (2005).
[48] P. Huerre and M. Rossi, in *Hydrodynamics and Nonlinear Instabilities*, edited by G. Godrèche and P. Manneville (Cambridge University Press, Cambridge, UK, 2005).
[49] M. d'Olce, J. Martin, N. Rakotomalala, D. Salin, and L. Talon, "Convective/absolute instability in miscible core-annular flow. Part 1: Experiments," J. Fluid Mech. **618**, 305 (2008).
[50] B. Selvam, L. Talon, L. Lesshafft, and E. Meiburg, "Convective/absolute instability in miscible core-annular flow. Part 2. Numerical simulations and nonlinear global modes," J. Fluid Mech. **618**, 323 (2008).
[51] O. Reynolds, "An experimental investigation of the circumstances which determine whether the motion of water shall be direct or sinuous, and of the laws of resistance in parallel channels," Philos. Trans. R. Soc., London **174**, 935 (1883).